Journal of Membrane Science 377 (2011) 249–260

Contents lists available at ScienceDirect

Journal of Membrane Science

journal homepage: www.elsevier.com/locate/memsci

# Investigating the potential of MgMOF-74 membranes for $CO_2$ capture

Rajamani Krishna*, Jasper M. van Baten

*Van 't Hoff Institute for Molecular Sciences, University of Amsterdam, Science Park 904, 1098 XH Amsterdam, The Netherlands*

ARTICLE INFO

*Article history:*
Received 4 March 2011
Received in revised form 20 April 2011
Accepted 3 May 2011
Available online 11 May 2011

*Keywords:*
Binding energy
Metal–organic framework
Membrane permeation
Diffusion selectivity
Correlations

ABSTRACT

MgMOF-74 is a metal–organic framework (MOF) with exposed metal cation sites that has one-dimensional 1.1 nm sized hexagonal-shaped channels. On the basis of information available in the published literature, it appears that MgMOF-74 has significant advantages over other MOFs, with respect to its uptake capacity for $CO_2$. The primary objective of the present communication is to investigate the performance of MgMOF-74 membranes in separating $CO_2/H_2$, $CO_2/N_2$, $CO_2/CH_4$, and $CH_4/H_2$ mixtures, that are important in carbon capture. To achieve this objective all the parameters required for modeling MgMOF-74 membrane permeation were obtained using molecular simulations. Specifically, Configurational-Bias Monte Carlo (CBMC) simulations were used to determine pure component adsorption isotherms, and isosteric heats of adsorption. Molecular dynamics (MD) simulations were performed to determine the self-diffusivities, $D_{i,self}$, and the Maxwell–Stefan ($M$–$S$) diffusivities, $Đ_i$, of guest molecules.

The MD simulations show that the zero-loading diffusivity $Đ_i(0)$ is consistently lower, by up to a factor of 10, than the values of the Knudsen diffusivity, $D_{i,Kn}$. The ratio $Đ_i(0)/D_{i,Kn}$ is found to correlate with the isosteric heat of adsorption, which in turn is a reflection of the binding energy for adsorption at the pore walls. The stronger the binding energy, the lower is the ratio $Đ_i(0)/D_{i,Kn}$.

Using the Maxwell–Stefan formulation for binary mixture permeation, along with data inputs from CBMC and MD simulations, the permeation selectivities for $CO_2/H_2$, $CO_2/N_2$, $CO_2/CH_4$, and $CH_4/H_2$ mixtures were determined for a range of upstream pressures. The model calculations show that increased upstream pressures lead to significant enhancement in permeation selectivities; this enhancement is directly traceable to diffusional correlations within the 1D channels. Such correlations have the effect of slowing-down the more mobile partner species in the mixtures.

MgMOF-74 membrane permeation selectivities for $CO_2/H_2$, and $CO_2/N_2$ mixtures are higher than those reported in the published literature with zeolite membranes.



## 1. Introduction

In recent years there has been considerable research on the development of novel porous materials such as metal–organic frameworks (MOFs) [1], and zeolitic imidazolate frameworks (ZIFs) [2,3]. MOFs, and ZIFs offer considerable potential for application in a wide variety of separation applications [4–10]. A substantial amount of the published research on metal–organic frameworks (MOFs) is dedicated to the issue of $CO_2$ capture by selective adsorption [6,9,11–14]. Of particular interest in $CO_2$ capture applications are MOFs with exposed metal cation sites such as MMOF-74 (=$M_2$(dobdc)) with M = Mg, Zn, Ni, or Co [15–20]. Yazaydın et al. [20] have screened a total of 14 different MOFs and ZIFs and concluded that MgMOF-74 has the highest $CO_2$ uptake capacity. For adsorption of $CO_2$ and $CH_4$, Bao et al. [21] have found significantly higher capacities for MgMOF-74 when compared to 13X zeolite. Furthermore, the $CO_2/CH_4$ adsorption selectivity for MgMOF-74 was found to be comparable to that of 13X zeolite. MgMOF-74 yields $CO_2/CH_4$ adsorption selectivities that are significantly higher than those reported for CuBTC in the experiments of Hamon et al. [22]. For separation of $CO_2/H_2$ mixtures, Herm et al. [23] compared the adsorption selectivities of five different MOFs: MgMOF-74, MOF-177, CuBTTri, BeBTB, and Co(BDP), with traditionally used adsorbents such as NaX. Their study concludes that while the adsorption selectivity of MgMOF-74 is higher than that of NaX, and has the additional advantage of having a significantly higher capacity. The molecular simulation studies of Gallo et al. [24] and Keskin [25], had concluded, respectively, that ZnMOF-74 and CoMOF-74 yield the highest adsorption selectivities values for $CH_4/H_2$ separation.

One technological solution is to allow the gaseous mixture to permeate through a porous crystalline layer, with a thickness of a few micrometers [13,25–33]. For the development of such membrane devices, it is essential to have information not only

* Corresponding author. Tel.: +31 20 6270 990; fax: +31 20 5255604.
*E-mail address:* r.krishna@uva.nl (R. Krishna).

0376-7388/$ – see front matter © 2011 Elsevier B.V. All rights reserved.
doi:10.1016/j.memsci.2011.05.001

on adsorption, but also on the diffusivities of the guest molecules inside the pores.

The primary objective of the present communication is to investigate the performance of MgMOF-74 membranes in separating $CO_2/H_2$, $CO_2/N_2$, $CO_2/CH_4$, and $CH_4/H_2$ mixtures, that are important in $CO_2$ capture. To achieve this objective all the parameters required for characterizing the permeation characteristics of MgMOF-74 membranes were obtained using molecular simulations. Specifically, Configurational-Bias Monte Carlo (CBMC) simulations were used to determine pure component adsorption isotherms, and isosteric heats of adsorption. Molecular dynamics (MD) simulations were performed to determine the diffusivities of guest molecules. Besides $H_2$, $N_2$, $CO_2$, and $CH_4$, we also investigated the diffusion characteristics of higher alkanes: ethane (C2), propane (C3), and n-butane (nC4) in order to establish a correlation between diffusivities and binding energies. Furthermore, for comparison purposes and to obtain a broader perspective on membrane permeation, the adsorption and diffusion characteristics of ZnMOF-74 [15,16,19,20], that is iso-structural with MgMOF-74, were also investigated.

Supplementary material accompanying this publication gives information on the specific force fields used, unit cell dimensions, accessible pore volume, characteristic pore dimensions, molecular simulation methodologies, pore landscapes and snapshots, along with the entire data base of simulation data on isotherms, heats of adsorption, and diffusivities.

## 2. Maxwell–Stefan model and diffusivities

For modeling of intra-crystalline mixture diffusion in membrane permeation devices it is commonly accepted that the fundamentally correct approach is to relate the fluxes $N_i$, defined in terms of the cross-sectional area of the membrane, to the chemical potential gradients by use of the Maxwell–Stefan ($M$–$S$) equations [34–36]

$$-\phi\frac{c_i}{RT}\frac{d\mu_i}{dz}=\sum_{\substack{j=1\\ j\neq i}}^{n}\frac{x_jN_i-x_iN_j}{Đ_{ij}}+\frac{N_i}{Đ_i};\quad i=1,2,\ldots,n \tag{1}$$

where $\phi$ represents the fractional pore volume of the porous material, and the concentrations $c_i$ are defined in terms of moles per $m^3$ of accessible pore volume. The $x_i$ in Eq. (1) is the component mole fractions of the adsorbed phase

$$x_i=\frac{c_i}{c_t};\quad i=1,2,\ldots,n \tag{2}$$

There are two kinds of diffusivities that are needed. Firstly we need information on the $Đ_i$, that characterize species $i$–wall interactions. In many cases the $Đ_i$ corresponds to the value of the pure component $i$; consequently this can be estimated from unary diffusion data. In some exceptional cases the $Đ_i$ in the mixture can be lower than that of pure components [37–39]. In the published literature there is only one experimental study, that reports the $M$–$S$ diffusivities of $CO_2$ and $CH_4$ in MgMOF-74 [21].

Secondly, we need data on the $Đ_{ij}$; these are exchange coefficients representing interaction between components $i$ with component $j$. At the molecular level, the $Đ_{ij}$ reflect how the facility for transport of species $i$ *correlates* with that of species $j$. Conformity with the Onsager reciprocal relations prescribes

$$Đ_{ij}=Đ_{ji} \tag{3}$$

The relative contributions of the first and second right members of Eq. (1) are dictated by the *degree of correlations*, defined as $Đ_i/Đ_{ii}$; the higher the degree of correlations, the more important is the contribution of the first right member. We will see later that correlation effects are of paramount importance in MgMOF-74 membrane permeation.

In earlier published formulations on multicomponent diffusion in zeolites and MOFs [40,41], the $M$–$S$ equations are set up differently using loadings, $q_i$, expressed as moles per kg of framework; the inter-relationship between $c_i$ and $q_i$ is

$$c_i=\frac{q_i}{V_p} \tag{4}$$

where $V_p$ is the accessible pore volume. For MgMOF-74 the value of $V_p$, obtained from molecular simulations using the helium probe insertion technique suggested by Talu and Myers [42,43], is 0.78 $cm^3/g$. Furthermore, the earlier formulations use fractional occupancies, $\theta_i$, defined by

$$\theta_i\equiv\frac{c_i}{c_{i,sat}} \tag{5}$$

in place of the adsorbed phase mole fractions, $x_i$. For a detailed comparison of the earlier approaches with the current one, using Eq. (1), see Supplementary material accompanying the paper of Krishna and Van Baten [34]. There are important advantages in using the current approach using moles per accessible pore volume, $c_i$. Firstly, Eq. (1), is applicable equally to micro- and meso-porous materials, as explained in our earlier papers [34,35,44–47]. Secondly, the use of the current formulation allows a much clearer interpretation of the $M$–$S$ diffusivities $Đ_{ij}$; these are relatable to the corresponding $M$–$S$ diffusivity in the *binary* fluid mixture [34,35].

The MD data on the $M$–$S$ diffusivities, $Đ_i$, for $H_2$, $N_2$, $CO_2$, $CH_4$, C2, C3, and nC4 diffusion in the 1D channels of MgMOF-74 are shown in Fig. 1a as a function of the pore concentrations, $c_i$. It is interesting to note that the hierarchy of $Đ_i$ values: $H_2 > N_2 > CH_4 > C2 > C3 \approx CO_2 \approx nC4$ does not appear to correlate with either the molar mass, $M_i$, or the kinetic diameter; this needs further investigation and analysis.

In the limit of vanishingly small loadings, $c_i \to 0$, the zero-loading diffusivity value $Đ_i(0)$ is dictated primarily by molecule-wall collisions. When the reflections are purely *diffuse* in nature, i.e. the angle of reflection bears no relation to the angle of incidence at which the molecule strikes the pore wall, the $Đ_i(0)$ value corresponds to that obtained by the classic Knudsen formula

$$D_{i,Kn}=\frac{d_p}{3}\sqrt{\frac{8RT}{\pi M_i}} \tag{6}$$

Eq. (6) holds in the limiting case when the molecule does not adsorb at pore walls [34,35,48–50].

MgMOF-74 has one-dimensional (1D) hexagonal-shaped channels; see Fig. 2. The effective channel diameter $d_p$ was determined following the method of Delaunay triangulation, described in the work by Foster et al. [51]. The maximum diameter of a sphere that can pass through the channels is determined to be 1.1 nm. Taking $d_p = 1.1$ nm, the application of Eq. (6) yields $D_{i,Kn} = 65 \times 10^{-8}\ m^2\ s^{-1}$, which value is slightly higher than the value of $Đ_i(0) \approx 55 \times 10^{-8}\ m^2\ s^{-1}$ obtained from MD. For ZnMOF-74, that has channel dimensions almost identical to that of MgMOF-74, we note that the $Đ_i(0)$ for $H_2$ is practically the same as the Knudsen value; see Fig. 2b. $H_2$ has a poor adsorption strength, and it is therefore not surprising that the diffuse reflectance assumption is a reasonable one, and the Knudsen prescription holds.

For species other than $H_2$, adsorption at the pore wall is significant, the values of $Đ_i(0)$ show considerable deviation from the values of $D_{i,Kn}$. For example, the diffusivity of $CO_2$ in MgMOF-74 is seen to be five times lower than that of $CH_4$, in excellent agreement with the value obtained in the experiments of Bao et al. [21]. However, on the basis of Eq. (6) we should expect this factor to be only lower by a factor $\sqrt{44/16} = 1.66$. In MgMOF-74 the values of $Đ_i(0)/D_{i,Kn}$ are 0.43, 0.25, 0.17, 0.108, 0.123, and 0.124 for $N_2$, $CH_4$,

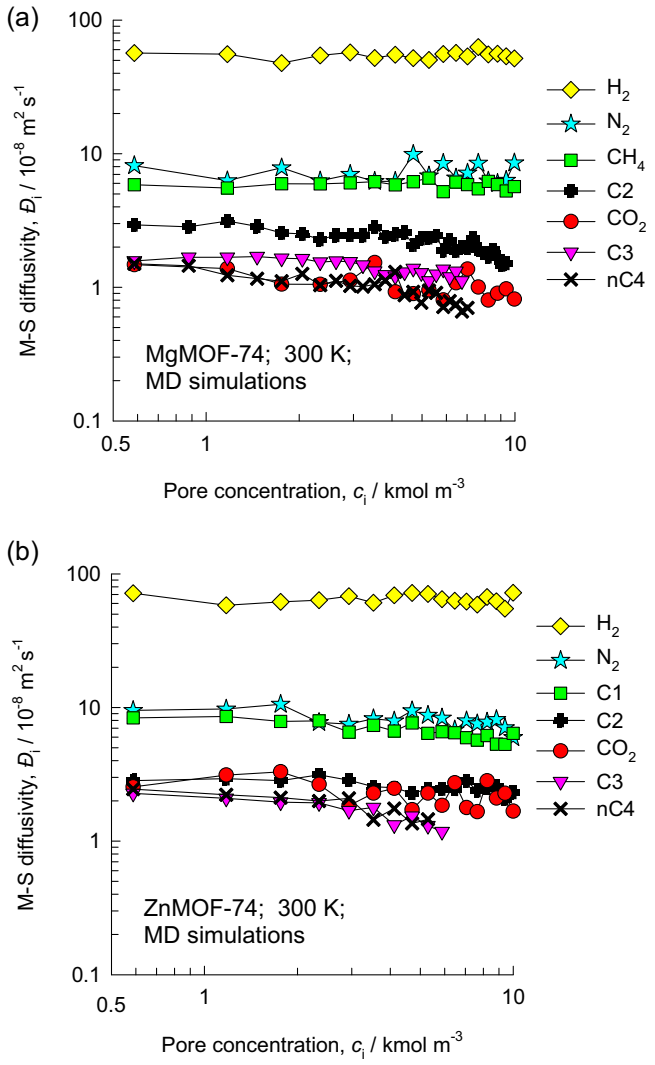


**Fig. 1.** MD simulations of *M–S* diffusivities, $Đ_i$, of $H_2$, $N_2$, $CO_2$, $CH_4$, C2, C3, and nC4 in the 1D channels of (a) MgMOF-74, and (b) ZnMOF-74 at 300 K, expressed as a function of the pore concentrations, $c_i$.

C2, $CO_2$, C3, and nC4, respectively. In ZnMOF-74 the corresponding values $Đ_i(0)/D_{i,Kn}$ values for these species are 0.49, 0.28, 0.24, 0.18, 0.18, and 0.174.

Let us examine whether the extent of departures from the Knudsen prescription correlates with the binding energy of the molecules. A measure of the binding energy is the isosteric heats of adsorption, $-\Delta H_{st}$. CBMC simulation data on $-\Delta H_{st}$ are presented in Fig. 3a and b for MgMOF-74 and ZnMOF-74 respectively. We note that $CO_2$ has the highest heat of adsorption, reflecting the strongest binding energy amongst all the investigated species. For MgMOF-74, the ratio $Đ_i(0)/D_{i,Kn}$ is seen to correlate well with the isosteric heat of adsorption; see Fig. 4a. This is a rational result; the higher the binding energy, the higher is the sticking tendency of that species with the pore wall, leading to greater departure from the Knudsen prescription of diffuse reflectance. It is also interesting to note that the $Đ_i(0)/D_{i,Kn}$ values tend to reach an asymptote value of about 0.1. The higher the binding energy the higher is the probability that a molecule hops to a neighboring adsorption site rather than return to the bulk gas phase after collision with the pore wall [35,49,52]. This bias is best appreciated by viewing video animations of MD simulations showing the hopping of $H_2$, $N_2$, $CH_4$, C2, C3, and nC4 within the 1D channel MgMOF-74; these Video animations have been provided as Supplementary material accompanying this publication. The trajectories followed by $H_2$ molecules, as seen in the animations, clearly show that a $H_2$ molecule that strikes the pore wall has a tendency to return to the bulk gas phase largely in keeping with the diffuse reflection scenario prescribed by the Knudsen theory. For all other species, the adsorption at the pore walls causes many molecules to jump to a neighboring site rather than return to the bulk gas phase.

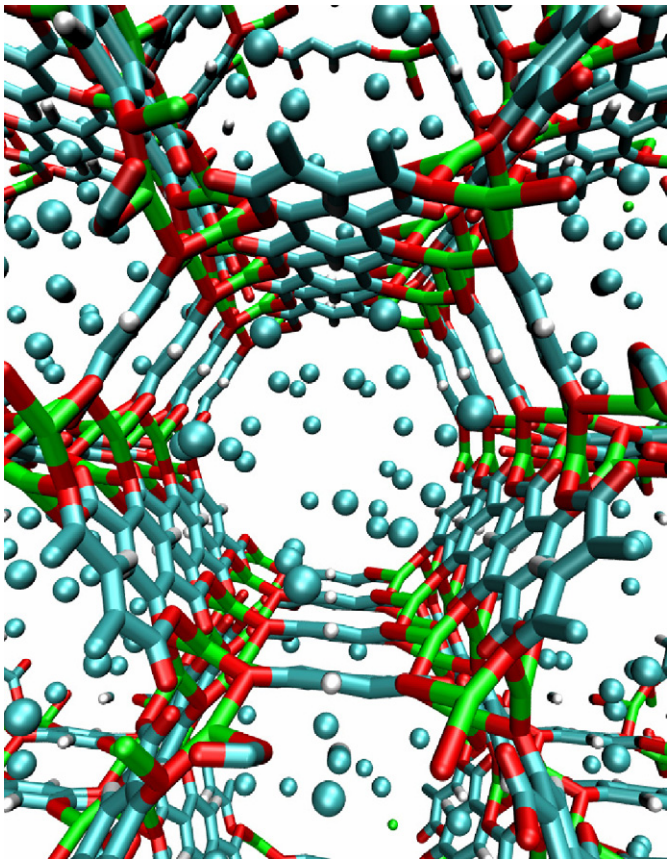

**Fig. 2.** Snapshots of adsorbed $CH_4$ molecules within the 1D channels of MgMOF-74.

Fig. 4b presents the corresponding correlation of the ratios $Đ_i(0)/D_{i,Kn}$ with the isosteric heats of adsorption for ZnMOF-74. In this case, the value of the ratio $Đ_i(0)/D_{i,Kn}$ for $CO_2$ is 0.18. This higher value as compared to MgMOF-74 is because of the lower binding energy of $CO_2$; this is reflected in the heat of adsorption value of 25 kJ mol$^{-1}$, compared to 32 kJ mol$^{-1}$ for MgMOF-74.

The information in Fig. 4 provides a practical methodology for estimation of the $Đ_i(0)$ using the $D_{i,Kn}$ value as a starting point.

## 3. Correlation effects, and diffusion selectivities

Applying Eq. (1) to a mixture of tagged and untagged species *i*, we can derive the following expression for the self-diffusivities, $D_{i,self}$, for unary diffusion [35]

$$\frac{1}{D_{i,self}} = \frac{1}{Đ_i} + \frac{1}{Đ_{ii}} \tag{7}$$

The self-exchange coefficients, $Đ_{ii}$, are starting points for the estimation of the $Đ_{ij}$. The ratio $Đ_i/Đ_{ii}$ is a measure of the *degree of correlations* for unary diffusion. Fig. 5a and b shows the MD simulated data for $D_{i,self}$, along with the ratio $Đ_i/Đ_{ii}$ for various guest molecules in MgMOF-74. For any species, the $Đ_i/Đ_{ii}$ increases with increasing pore concentration, $c_i$. As the concentration within the pores increases, the jumps of individual molecules become increasingly correlated because the number of vacant adsorption sites will

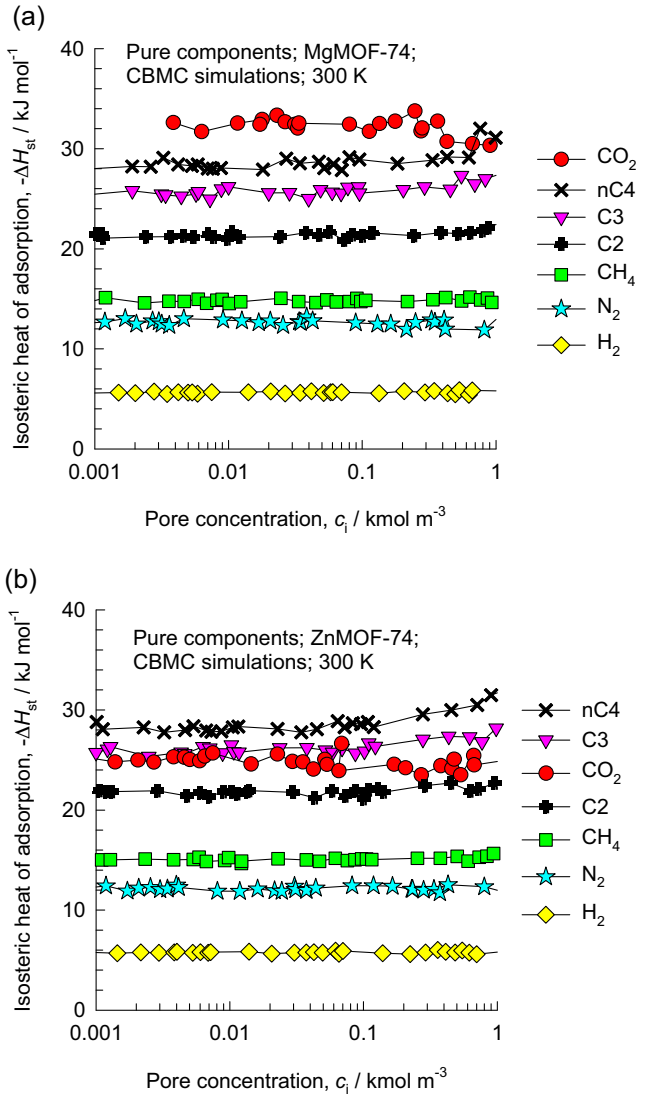


**Fig. 3.** CBMC simulation data on the isosteric heats of adsorption, $-\Delta H_{st}$, in (a) MgMOF-74, and (b) ZnMOF-74 of $H_2$, $N_2$, $CO_2$, $CH_4$, C2, C3, and nC4 at 300 K.

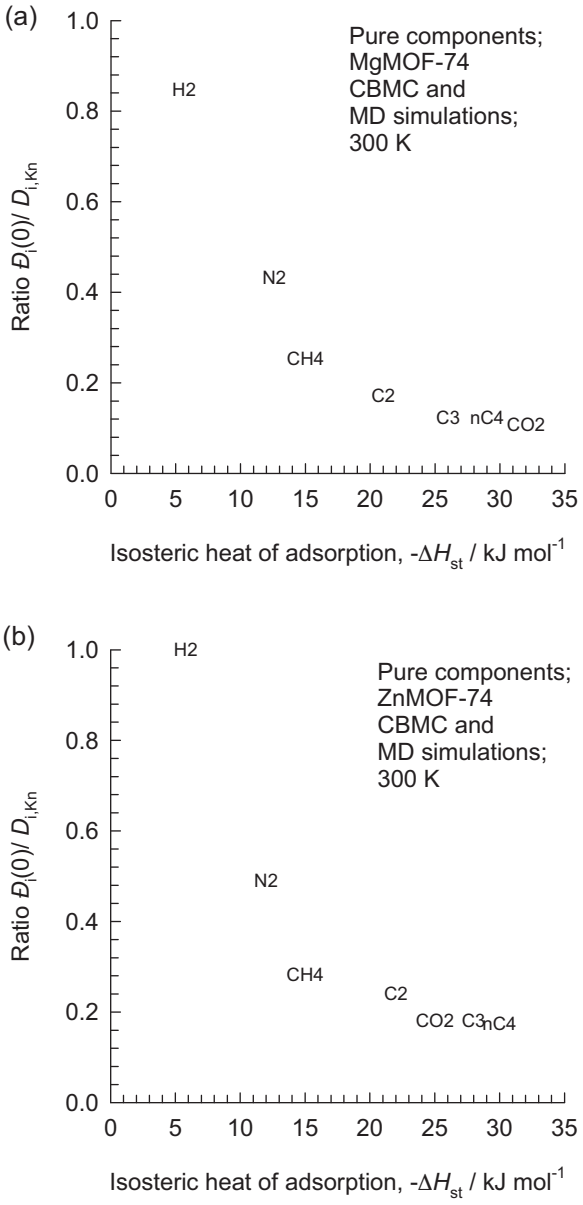


**Fig. 4.** The ratio of $Đ_i$ to the Knudsen diffusivity, $Đ_i(0)/D_{i,Kn}$, for (a) MgMOF-74, and (b) ZnMOF-74, plotted as function of the isosteric heat of adsorption $-\Delta H_{st}$ of the corresponding species.

decrease, and the probability of unsuccessful jumps will increase. Fig. 5c compares the degree of correlations for methane diffusion in a variety of zeolites and MOFs. The strongest degree of correlations are within the 0.74 nm sized 1D channels of MIL-53(Cr). The degree of correlations in MgMOF-74, are similar to that of ZnMOF-74, and both are comparable with those found for the intersecting channels of MFI zeolite. Published MD simulations also show that the inter-cage hopping of molecules across the narrow windows of DDR, CHA, LTA, and ITQ-29 zeolites is practically uncorrelated, and a good approximation is to take $Đ_i/Đ_{ii} \approx 0$ for such structures [38,40,41].

It is worth pointing out here that in our earlier work on the development of the *M–S* equations for micropore diffusion we had suggested the approximation $Đ_i/Đ_{ii} \approx 1$ [53,54]. Subsequently, MD simulation results became available to show the $Đ_i/Đ_{ii}$ varies with pore concentrations for all guest-host combinations [40,55]. It is remarkable, therefore, to note that the recent paper by Lito et al. [56] invokes the assumption $Đ_i/Đ_{ii} = 1$ to describe diffusion across both MFI membranes. As seen from the data in Fig. 5c, and in the extensive MD simulation results for MFI presented earlier [40,55], $Đ_i/Đ_{ii}$ for guest molecules such as $CO_2$, and linear alkanes in MFI increases significantly with pore concentration. The permeation calculations of Lito et al. [56] must therefore be viewed with caution. Indeed, an important message that emerges later in this paper is that the *increase* in the degree of correlations with pore concentrations is a key to the success of MgMOF-74 membrane separations.

For mixture diffusion, correlations in molecular jumps have the effect of slowing down the more mobile species because the tardier species does not vacate the adsorption site quick enough. In order to demonstrate the slowing down effect let us consider diffusion in binary mixture $CO_2(1)/H_2(2)$ with equal concentrations, i.e. $c_1 = c_2$. The slowing-down effect is quantified by the diffusion selectivity, $S_{diff}$. Starting with the *M–S* Eq. (1) the following expression for $S_{diff}$ can be derived [13]

$$S_{diff} = \frac{Đ_1}{Đ_2}\frac{1+(Đ_2/Đ_{12})}{1+(Đ_1/Đ_{12})} \tag{8}$$

The derivation of Eq. (8) is provided in Supplementary material, along with an explanation on how MD mixture simulations are

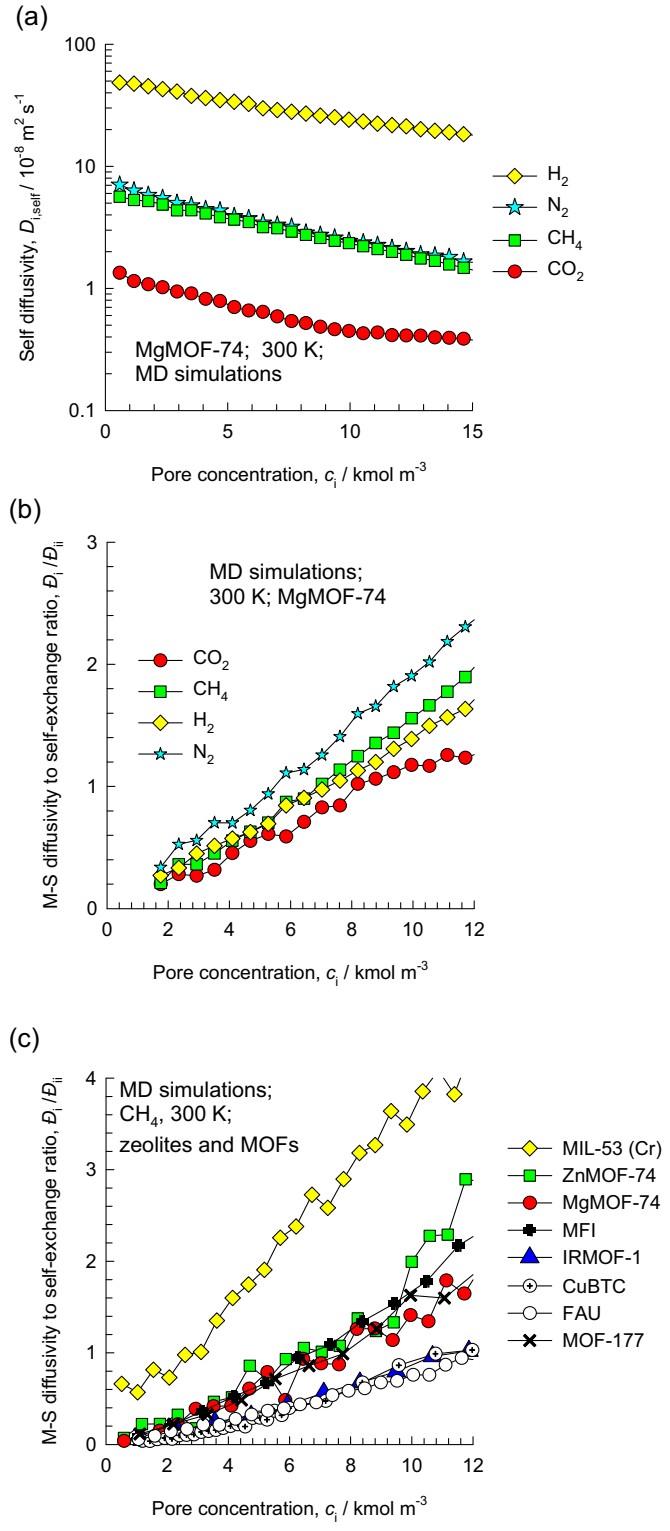


**Fig. 5.** MD simulations of (a) self-diffusivities $D_{i,self}$, and (b) the degree of correlations, $Đ_i/Đ_{ii}$, for diffusion of $H_2$, $N_2$, $CO_2$, $CH_4$, C2, C3, and nC4 in the 1D channels of MgMOF-74 at 300 K, expressed as a function of the pore concentrations, $c_i$. (c) Comparison of the degree of correlations, $Đ_i/Đ_{ii}$, for diffusion of $CH_4$ in a variety of zeolites (MFI, FAU) and MOFs (IRMOF-1, CuBTC, MIL-53(Cr), MOF-177, MgMOF-74) at 300 K, expressed as a function of the pore concentrations, $c_i$.

used for the calculations. As an approximation, and for screening purposes, the right member of Eq. (8) is often assumed to be equal to the ratio of the self-diffusivities $D_{i,self}$ in the mixture [13,49,50]

$$S_{diff} = \frac{D_{1,self}}{D_{2,self}} \tag{9}$$

Eq. (9) is a reasonable approximation when the pore concentrations significantly lower than those corresponding to saturation conditions. For MgMOF-74, the $CO_2$ adsorption strength is high and this approximation is not a good one to use.

For a variety of MOFs, the right member of Eq. (8), determined from $CO_2/H_2$ mixture simulations, are plotted in Fig. 6a as a function of the total pore concentration, $c_t$. Also plotted in Fig. 6a is the value of the Knudsen selectivity

$$\frac{D_{1,Kn}}{D_{2,Kn}} = \sqrt{\frac{M_2}{M_1}} \tag{10}$$

For all the MOFs, the $S_{diff}$ is lower the Knudsen selectivity at low pore concentrations; this is because $CO_2$ has a significantly higher binding energy than $H_2$. Indeed, the hierarchy of values of $S_{diff}$ in Fig. 6a is inverse to the hierarchy of the isosteric heats of adsorption of $CO_2$ in the corresponding MOFs; cf. Fig. 6b. The stronger the binding energy of $CO_2$, the lower is the diffusion selectivity. With increasing pore concentration, the correlations become stronger. This has the effect of slowing down the more mobile $H_2$; consequently $S_{diff}$ increases with increasing $c_t$. It is noteworthy that with increasing degree of correlations, the Knudsen selectivity value can be exceeded.

Fig. 7a and b presents data on the diffusion selectivity for diffusion of $CO_2/N_2$, and $CO_2/CH_4$ mixtures in MgMOF-74 and ZnMOF-74. For both mixtures, $S_{diff}$ for MgMOF-74 is significantly lower than for ZnMOF-74, due to the higher binding energy of $CO_2$. For $CH_4/H_2$ mixture diffusion the $S_{diff}$ values in MgMOF-74 and ZnMOF-74 are the same; see Fig. 7c. This is because the binding energies of $CH_4$ are practically identical in these two MOFs.

The data presented in Figs. 6 and 7 lead to the inescapable conclusion that the adsorption selectivity does not go hand in hand with diffusion selectivity. This conclusion is generally valid for "open" microporous materials such as zeolites, MOFs, and ZIFs that have pore sizes larger than about 0.74 nm [13,14,35]. For structures such as LTA, CHA, DDR, and ZIF-8 that have cages separated by narrow windows in the 0.35–0.41 nm size range, it is possible to have the diffusion and adsorption selectivities complement each other [40,57].

## 4. Membrane permeation

We now consider permeation of (a) $CO_2(1)/H_2(2)$, (b) $CO_2(1)/N_2(2)$, (c) $CO_2(1)/CH_4(2)$, and (d) $CH_4(1)/H_2(2)$ mixtures across a MgMOF-74 membrane with microporous crystalline layer of thickness $l = 50\,\mu m$. The microporous layer consists of pure MOF-74 crystals, without any supporting matrix polymer. There is however a practical issue relating to the orientation, and alignment of all the 1D channels. For the purposes of the calculations presented here, it is assumed that all the crystals are aligned in such a way that the 1D channels are parallel to the direction of gas flow. For all mixtures the species 1 has the higher adsorption strength, while the species 2 has higher diffusivity.

The first step is to re-write the chemical potential gradients in Eq. (1) in a more practically usable form. The chemical potential gradients can be related to the more conventional gradients of con-

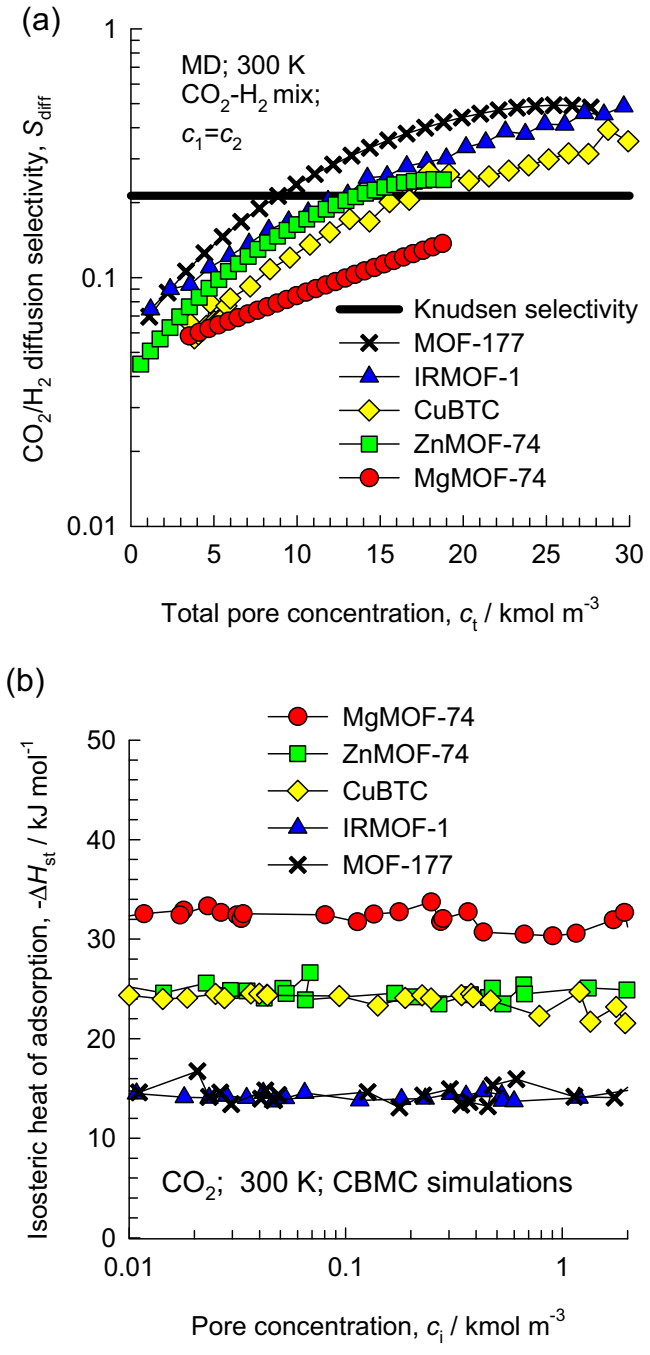


**Fig. 6.** (a) The diffusion selectivity, $S_{diff}$, for equimolar ($c_1 = c_2$) $CO_2/H_2$, mixtures in MgMOF-74, ZnMOF-74, MOF-177, IRMOF-1, and CuBTC at 300 K, plotted as a function of the total pore concentration, $c_t = c_1 + c_2$. (b) CBMC simulation data on the isosteric heats of adsorption, $-\Delta H_{st}$ of $CO_2$ in various MOFs plotted against the pore concentrations, $c_i$. The MD data for MOF-177, IRMOF-1, and CuBTC are from earlier work [13].

centrations within the pores by defining thermodynamic correction factors $\Gamma_{ij}$

$$\frac{c_i}{RT}\frac{d\mu_i}{dz} = \sum_{j=1}^{2}\Gamma_{ij}\frac{dc_j}{dz}; \qquad \Gamma_{ij} = \frac{c_i}{p_i}\frac{\partial p_i}{\partial c_j}; \quad i,j = 1,2 \tag{11}$$

For determination of the adsorbed phase pore concentrations $c_i$ and the elements $\Gamma_{ij}$, in the binary mixtures, the Ideal Adsorbed Solution Theory (IAST) of Myers and Prausnitz [58] was used. For application of the IAST, pure component isotherm fits are required.

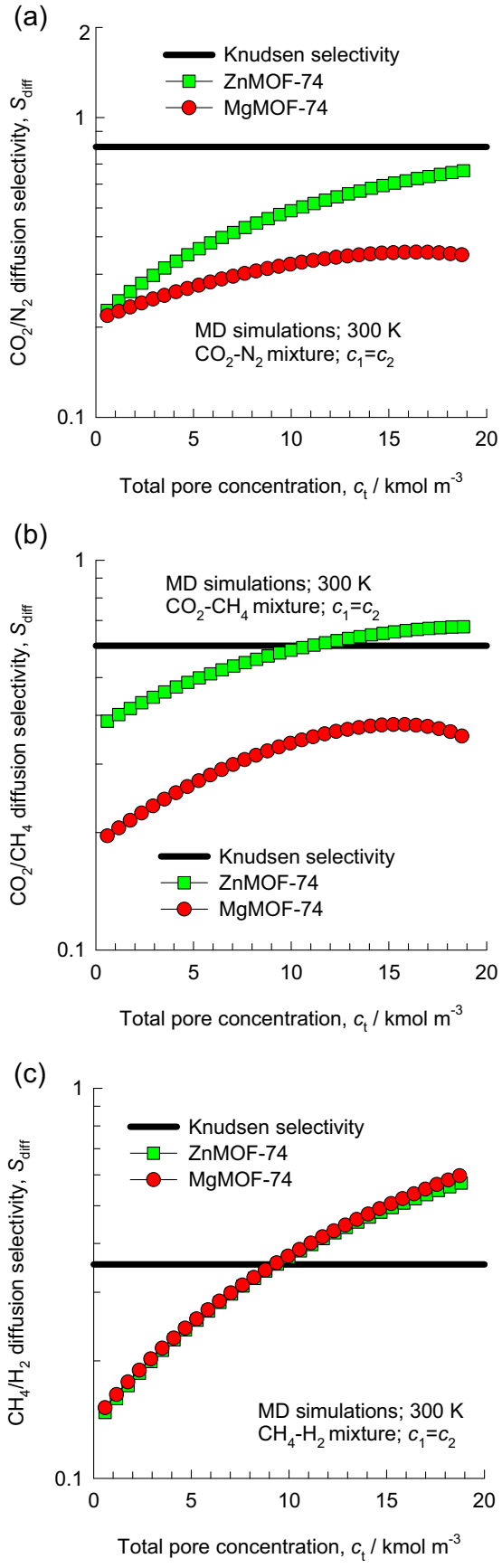


**Fig. 7.** The diffusion selectivity, $S_{diff}$, for equimolar ($c_1 = c_2$) (a) $CO_2/N_2$, (b) $CO_2/CH_4$, and (c) $CH_4/H_2$ mixtures in MgMOF-74 and ZnMOF-74 at 300 K, plotted as a function of the total pore concentration, $c_t = c_1 + c_2$.

For this purpose the dual-site Langmuir fits of the CBMC simulated pure component isotherms were employed; see Fig. 8a. In order to verify the accuracy of IAST calculations, we carried out CBMC simulations for $CO_2/N_2$, and $CO_2/H_2$ mixtures. Fig. 8b and c presents comparisons of the IAST predictions with the CBMC simulation data for component loadings. We see excellent agreement of the IAST with CBMC data; this confirms the applicability of IAST for practical purposes. Similar good agreement was earlier established for adsorption of a wide variety of mixtures in different zeolites [59,60].

In view of the fact that the accuracy of the CBMC simulations of the adsorption isotherms, especially of $CO_2$, are essential to the prediction of the permeation characteristics, we compare CBMC simulations of $CO_2$ isotherms at 300 K, and 313 K with the experimental results of Dietzel et al. [18] and Herm et al. [23]; see Fig. 9a and b. For both temperatures, the experimental data show an inflection at a loading of about 8 mol/kg that corresponds to one molecule of 1 $CO_2$ per atom of Mg in the framework. We note that for pressures exceeding 0.1 MPa, there is excellent agreement between the CBMC simulations and experiment. However, for pressures below 0.1 MPa, the experimental loadings are significantly higher than the simulated values. The reason for this deviation at pressures below 0.1 MPa can be traced to the fact that our force field implementation, following the work of Yazaydın et al. [20] does not explicitly account for orbital interactions and polarization. Such effects are particularly strong in the low pressure region; the influence of polarization is of lesser importance at higher pressures. Put another way, we would expect the CBMC simulation results to be reasonably good for high pressure membrane operation with upstream pressures that are considerably in excess of 0.1 MPa.

When the guest species do not have orbital interactions with the Mg atoms, the predictions of the CBMC simulations can be expected to be good. Fig. 9c compares CBMC simulations of the adsorption isotherms for $CH_4$ at 300 K with the experimental data of Dietzel et al. [18]; the agreement between the two sets is good for the entire pressure range.

An important consequence of the under-prediction of the $CO_2$ loadings for pressures below 0.1 MPa, is that the estimations of the adsorption selectivity from CBMC simulations can be expected to be conservative. To confirm this expectation, we compare the calculations of the adsorption selectivity for separation of 20/80 $CO_2/H_2$ mixtures using MgMOF-74 in the experimental study of Herm et al. [23] with corresponding CBMC mixture simulations; see Fig. 9d. We note that the CBMC mixture simulations predict somewhat lower values of $S_{ads}$ over the range of pressures 0.1–10 MPa. On the basis of the results presented in Fig. 9d we conclude that the permeation selectivity results to be presented below are likely to be conservative.

At steady-state, the fluxes $N_i$ obey

$$\frac{\partial N_i}{\partial z} = 0 \tag{12}$$

The steady state permeation fluxes $N_i$ were determined by solving the set of Eqs. (1), (11) and (12) subject to the boundary conditions

$$\begin{aligned} z = 0; \quad p_i = p_{i0}; \quad c_i = c_{i0} \\ z = \ell; \quad p_i = p_{i\ell}; \quad c_i = c_{i\ell} \end{aligned} \tag{13}$$

using the numerical procedures described in our earlier works [54,61,62].

The $M$–$S$ diffusivities $Đ_i$ were taken from the data presented in Fig. 1a. The binary exchange coefficient $Đ_{12}$, in the mixtures were estimated on the basis of the pure component self-exchange coefficients, $Đ_{ii}$, using the interpolation formula [34,36]

$$Đ_{12} = (Đ_{11})^{x_1}(Đ_{22})^{x_2} \tag{14}$$

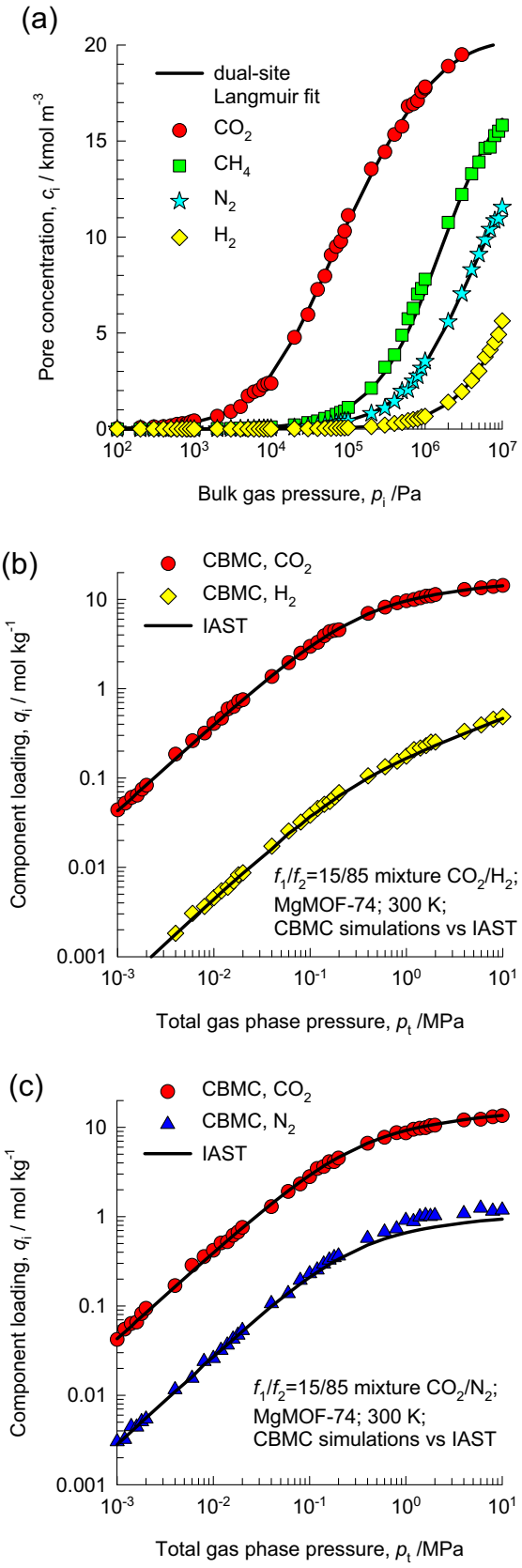


**Fig. 8.** (a) CBMC simulation data on the pure component adsorption isotherms of $H_2$, $N_2$, $CH_4$, and $CO_2$ in MgMOF-74 at 300 K. The continuous solid lines are the dual-Langmuir fits of the isotherms; the fit parameters are provided in Supplementary material accompanying this publication. (b, c) CBMC simulations for component loadings in $CO_2/N_2$, and $CO_2/H_2$ mixtures at 300 K with partial pressure $p_1/p_2 = 15/85$. The continuous solid lines are the IAST calculations using the dual-Langmuir fits of the CBMC simulated pure component isotherms.

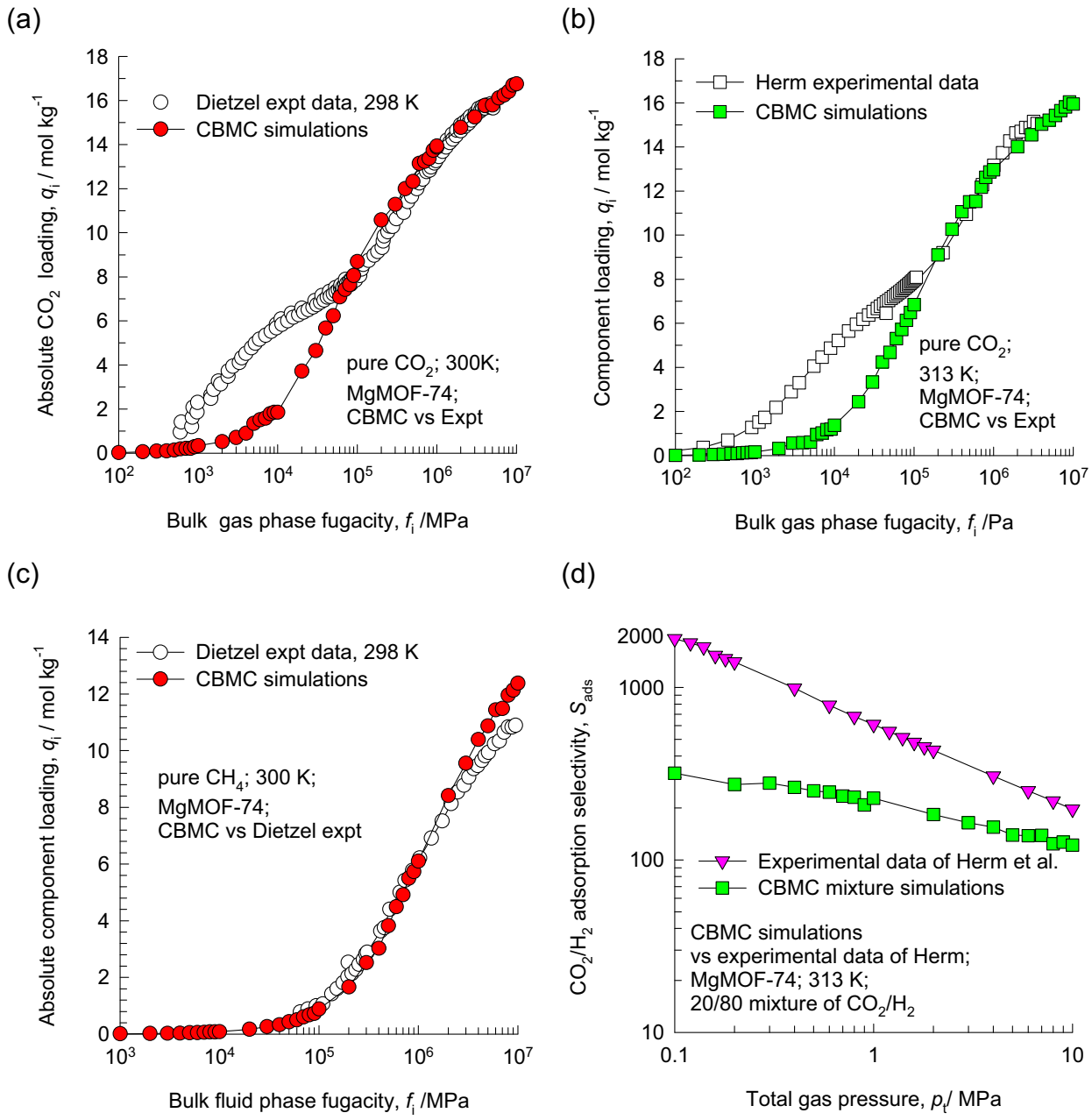


**Fig. 9.** (a, b) Comparison of the CBMC simulations of the pure component adsorption isotherms for $CO_2$ in MgMOF-74 at (a) 300 K, and (b) 313 K with experimental data of Dietzel et al. [18] and Herm et al. [23]. The published experimental data of Dietzel et al. is given in terms of excess loadings; these have been converted to absolute loadings by estimating the fluid densities within the pores using the Peng–Robinson equation of state. The experimental data on pore volume, 0.63 $cm^3/g$ was used in this conversion. (c) Comparison of the CBMC simulations of the pure component adsorption isotherms for $CH_4$ in MgMOF-74 at 300 K with experimental data of Dietzel et al. [18]. (d) Adsorption selectivity, $S_{ads}$, for 20/80 $CO_2/H_2$ mixture separation with MgMOF-74 at 313 K. Comparison of the experimental data of Herm et al. [23] with CBMC mixture simulations.

The data on $Đ_{ii}$ were obtained by fitting the $Đ_i/Đ_{ii}$ data plotted in Fig. 5b. All the data inputs are specified in the Supplementary material accompanying this publication.

Fig. 10 shows the calculations of the permeation selectivity, $S_{perm}$ defined by

$$S_{perm} = \frac{N_1/N_2}{p_{10}/p_{20}} \tag{15}$$

where $p_{i0}$ are the partial pressures in the upstream compartment. Also shown in Fig. 10 are IAST calculations of the adsorption selectivity, $S_{ads}$

$$S_{ads} = \frac{c_{10}/c_{20}}{p_{10}/p_{20}} \tag{16}$$

where $c_{i0}$ are the adsorption phase concentrations at the upstream face.

For all four mixtures, $S_{ads}$ either decreases with increasing upstream pressure ($CO_2/H_2$, and $CO_2/CH_4$), or remains practically constant ($CO_2/N_2$, and $CH_4/H_2$). It is remarkable, therefore, to note that $S_{perm}$ is significantly increased with $p_{t0}$ for all mixtures. This increase is directly attributable to the increase in the degree of correlations with increased loadings within the membrane. Put another way, with increased upstream pressure, the slowing-down effect is enhanced, resulting in a higher permeation selectivity. To underline this, Fig. 10 also presents the diffusion selectivity values, back-calculated using $S_{diff} = S_{perm}/S_{ads}$. The slowing-down effect is particularly dramatic for $CO_2/H_2$ mixtures. Here the $S_{diff}$ increases from 0.04 to a value approaching 0.7 at $p_{t0} > 1$ MPa. For the other

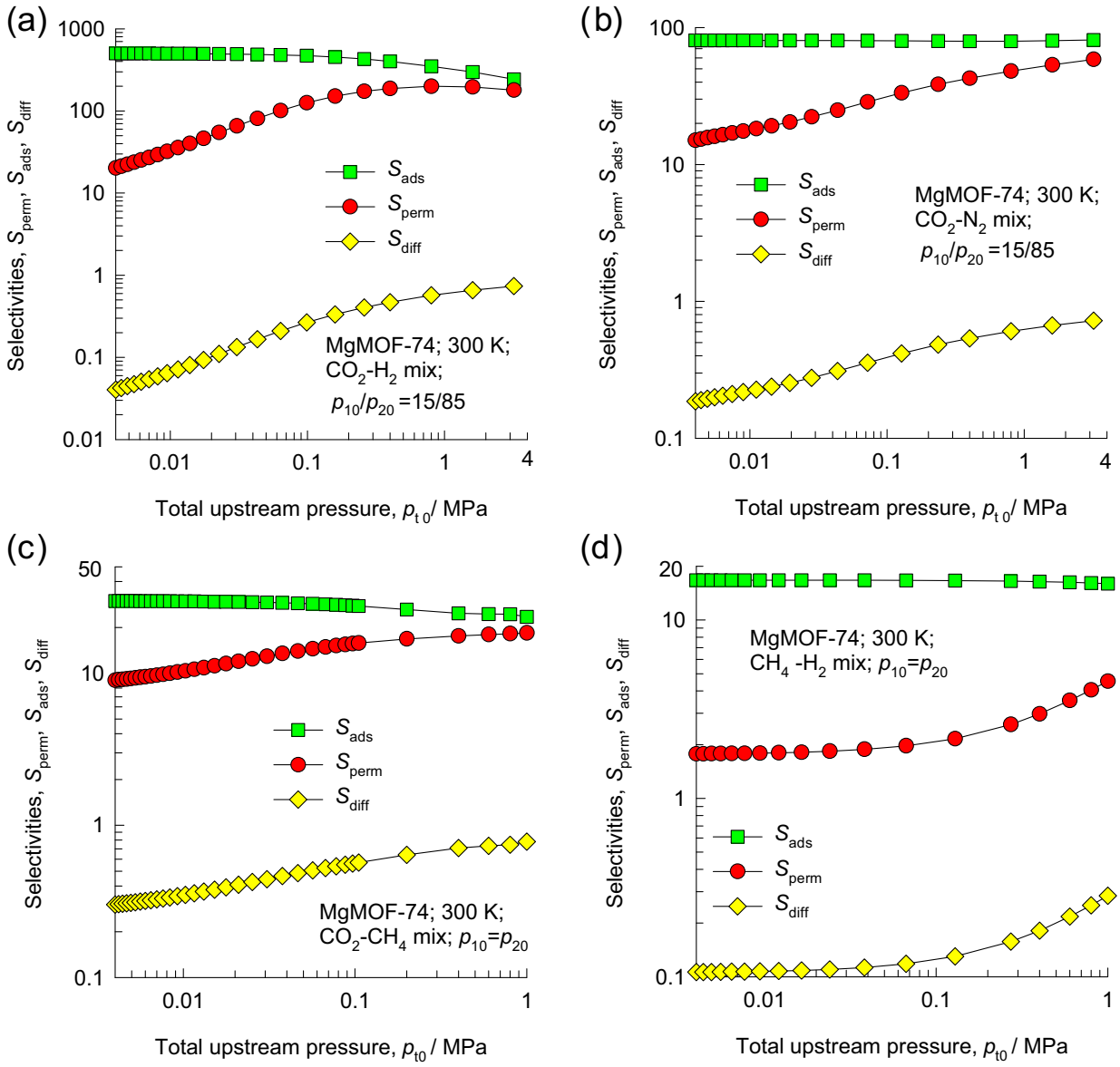


**Fig. 10.** Calculations for membrane permeation selectivity, $S_{perm}$, adsorption selectivity, $S_{ads}$, and diffusion selectivity, $S_{diff}$, for (a) $CO_2/H_2$, (b) $CO_2/N_2$, (c) $CO_2/CH_4$, and (d) $CH_4/H_2$ mixtures across a MgMOF-74 membrane at 300 K, plotted as a function of the total upstream pressure, $p_{t0} = p_{10} + p_{20}$. For (a) and (b) the partial pressures in the gas phase in the upstream compartment satisfy $p_{10}/p_{20} = 15/85$. In (c) and (d) $p_{10} = p_{20}$. The downstream partial pressures were maintained at 100 Pa for each species in all cases. The fractional porosity of the crystalline layer, $\phi = 0.708$. The thickness of MgMOF-74 crystalline layer, $l = 50\ \mu m$. The data on diffusivities, correlations, and dual-site Langmuir parameters for fitting of the pure component isotherms are specified in the Supplementary material accompanying this publication. The diffusion selectivities, $S_{diff}$, are obtained by dividing the $S_{perm}$ values by $S_{ads}$.

three mixtures the increase in $S_{diff}$ with increasing $p_{t0}$, though significant, is less dramatic.

The $S_{diff}$ values for all mixtures presented in Fig. 10 are seen to be higher than the corresponding values presented in Figs. 6 and 7. The reasoning is that the data in Figs. 6 and 7 are for equimolar ($c_1 = c_2$) mixtures, whereas the concentrations within the membrane are such that $c_1 \gg c_2$, i.e. containing a preponderantly higher proportion of the tardier species 1. To illustrate this, Fig. 11 presents the profiles of pore concentrations of $CO_2$ and $H_2$ within the 50 μm thick MgMOF-74 layer for permeation of $CO_2/H_2$ mixture with a total upstream pressure of 1 MPa. We note that $H_2$ amounts to less than 2% of the total mixture concentration. This small proportion of the more mobile $H_2$ gets severely retarded in its motion within the channels.

The $S_{perm}$ values of 200 estimated for $CO_2/H_2$ mixture at $p_{t0} > 1$ MPa, are more than an order of magnitude higher than those obtained in the experiments of Li et al. [63,64] for SAPO-34 membranes. For $CO_2/N_2$ mixtures, the estimated values of $S_{perm} > 40$ at $p_{t0} > 1$ MPa, are comparable to those reported by White et al. [65] for NaY membranes, and about a factor two higher than those obtained for SAPO-34 [63,64] and DDR [66] membranes.

There is a severe drawback to the use of SAPO-34 and DDR membranes that arises because of the severe constraint at the window regions; this restriction leads to significantly lower membrane permeances, defined by

$$\Pi_i \equiv \frac{N_i}{p_{i0} - p_{i\ell}} \tag{17}$$

Fig. 12 compares the permeances of $CO_2$ for $CO_2/H_2$ mixture permeation across MgMOF-74 and SAPO-34 membranes at 300 K. The $\Pi_i$ values of SAPO-34 are more than two orders of magnitude lower because the severe constraint for inter-cage jumps across the 0.38 nm × 0.42 nm sized windows of SAPO-34. When the window

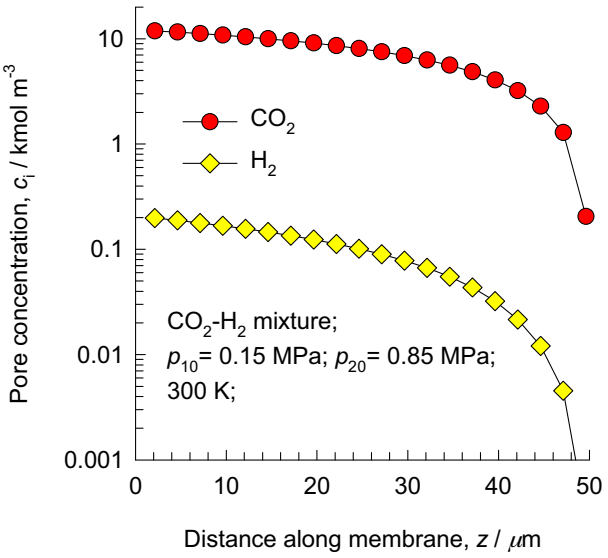


**Fig. 11.** Steady-state profiles of pore concentrations of $CO_2$ and $H_2$ within the 50 μm thick MgMOF-74 layer for permeation of $CO_2/H_2$ mixture. The upstream partial pressures are $p_{10}$ = 0.15 MPa, $p_{20}$ = 0.85 MPa.

size is still smaller, such as for ZIF-7 with 0.34 nm apertures, the mixture permeation is $H_2$-selective [67].

For $CO_2/CH_4$ mixtures the $S_{perm}$ value of 20 at $p_{t0}$ = 1 MPa, is significantly higher than those reported in the experiments of Bux et al. [32] for ZIF-8; however, this value is significantly lower than the reported values of $S_{perm} \approx 50$ for SAPO-34 [63,64] and $S_{perm}$ = 300 – 500 for DDR [66]. The narrow windows separating the cages of SAPO-34 and DDR membranes cause $CH_4$ to be severely constrained at the window regions, leading to $S_{diff}$ values exceeding 100 [38,41]. In other words, the higher $S_{perm}$ values for $CO_2/CH_4$ with SAPO-34 and DDR membranes are driven by diffusion selectivity.

The severe constraint experienced by $CH_4$ at the window regions of DDR, SAPO-34, ZIF-7, and ZIF-8 causes $CH_4/H_2$ mixture permeation to be $H_2$-selective [13,33,63,64,67,68].

The higher permeance of MgMOF-74, coupled with its significantly high permeation selectivity are both attractive features

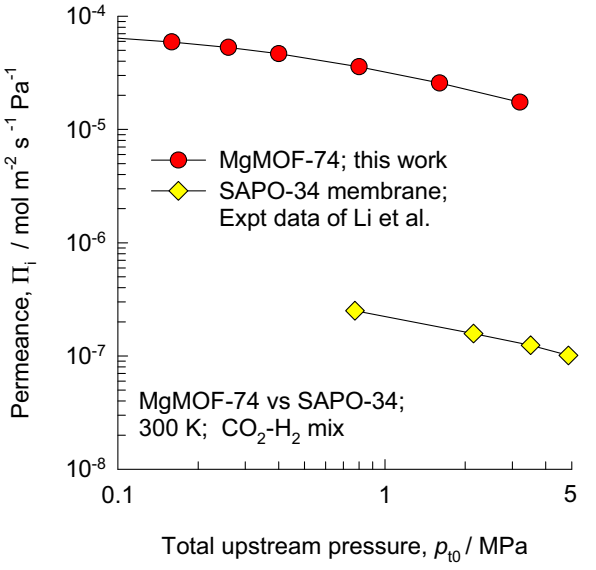


**Fig. 12.** Comparison of the permeances of $CO_2$ for $CO_2/H_2$ mixture permeation across MgMOF-74 and SAPO-34 membranes at 300 K.

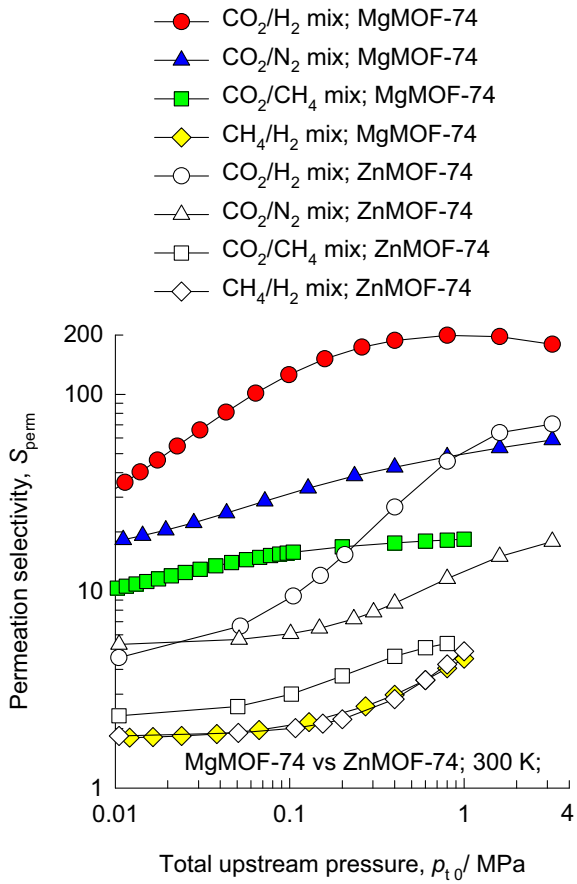


**Fig. 13.** Comparison of the permeation selectivity, $S_{perm}$, for $CO_2/H_2$, $CO_2/N_2$, $CO_2/CH_4$, and $CH_4/H_2$ mixtures across MgMOF-74 and ZnMOF-74 membranes. The upstream conditions are as in the legend to Fig. 10.

that warrant experimental verification for further technological exploitation, especially for $CO_2/H_2$, and $CO_2/N_2$ mixtures.

Finally, it is instructive to compare the selectivities for mixture permeation across MgMOF-74 and ZnMOF-74 membranes; see data in Fig. 13. For $CH_4/H_2$ mixtures, the permeation selectivities across MgMOF-74 and ZnMOF-74 membranes are practically the same; this is because the adsorption strengths of the $CH_4$ are practically the same in these structures, as is evidenced in similar values of the isosteric heats of adsorption; cf. Fig. 3a and b. Indeed, the obtained $S_{perm}$ values in the range of 2–4 for $CH_4/H_2$ mixtures were also obtained by Keskin [25] with CoMOF-74 and NiMOF-74 membranes. For $CO_2/H_2$, $CO_2/N_2$, and $CO_2/CH_4$ mixtures, the $S_{perm}$ values for MgMOF-74 are significantly higher than those for ZnMOF-74; the reason can be traced to the significantly higher binding energy of $CO_2$ in MgMOF-74 The higher diffusion selectivities of ZnMOF-74, witnessed in Figs. 6 and 7, cannot compensate for the significantly lower $S_{ads}$. MgMOF-74 is the membrane of choice for $CO_2$-selective permeation.

## 5. Conclusions

Molecular simulations have been used to investigate the characteristics of adsorption, and diffusion characteristics of a variety of guest molecules within the 1.1 nm channels of MgMOF-74. The following major conclusions can be drawn from this study.

With increasing binding energy of the guest molecules, the zero-loading diffusivity $Đ_i(0)$ falls increasingly below that predicted by the Knudsen formula, Eq. (6). The validity of Eq. (6) is restricted to

cases where the binding energy of the molecule is negligibly small, as is the case with $H_2$.

The ratio $Đ_i(0)/Đ_{i,Kn}$ for a given molecule correlates with the isosteric heat of adsorption; see Fig. 4. This correlation provides a good starting point for estimation of diffusivities.

The degree of correlations in molecular motions, $Đ_i/Đ_{ii}$, increases as the pore concentration increases; see Fig. 5.

For binary mixtures, the diffusion selectivity $S_{diff}$ is lower than the Knudsen formula when species 1 has the higher binding energy; see Fig. 5.

For binary mixtures in which species 2 is more mobile, $S_{diff}$ increases with increasing pore concentration due to increased correlation effects; see Figs. 6 and 7.

Adsorption and diffusion do not go hand in hand; the membrane permeation selectivity for binary mixtures $S_{perm}$ is significantly lower than $S_{ads}$; see Fig. 10.

For permeation of $CO_2/H_2$, $CO_2/N_2$, $CO_2/CH_4$, and $CH_4/H_2$ mixtures across a MgMOF-74 membrane, slowing-down effects become increasingly important at high upstream pressures, and consequently the $S_{perm}$ is significantly enhanced, and tends to approach $S_{ads}$ at $p_{t0} > 1$ MPa.

$CO_2/N_2$ permeation selectivities with MgMOF-74 membranes at $p_{t0} > 1$ MPa are about a factor two higher than those reported for SAPO-34 and DDR membranes.

Correlation effects are particularly important for $CO_2/H_2$ permeation, $S_{perm}$ values of 200 at $p_{t0} > 1$ MPa are more than an order of magnitude higher than those reported for SAPO-34 membrane.

An important advantage of MgMOF-74 membranes is that due to the 1.1 nm channel sizes, the permeances are more than two orders of magnitude higher than for SAPO-34 and DDR membranes.

Another message that emerges from this study is that Maxwell–Stefan modeling of membrane permeation fluxes must take proper account of diffusion correlations. For more accurate modeling of membrane permeation, there may be a need to also account for inter-crystalline and grain boundary resistances in the polycrystalline membrane layers.

## Acknowledgements

This material is based upon work supported as part of the Center for Gas Separations Relevant to Clean Energy Technologies, an Energy Frontier Research Center funded by the U.S. Department of Energy, Office of Science, Office of Basic Energy Sciences under Award Number DE-SC0001015.

## Appendix A. Supplementary data

Supplementary data associated with this article can be found, in the online version, at doi:10.1016/j.memsci.2011.05.001.

## Nomenclature

| | |
|---|---|
| $c_i$ | pore concentration of species $i$, mol m$^{-3}$ |
| $c_{i,sat}$ | saturation capacity of species $i$, mol m$^{-3}$ |
| $c_t$ | total concentration in mixture, mol m$^{-3}$ |
| $d_p$ | pore diameter, m |
| $D_{i,self}$ | self-diffusivity of species $i$, m$^2$ s$^{-1}$ |
| $Đ_i$ | Maxwell–Stefan diffusivity, m$^2$ s$^{-1}$ |
| $Đ_i(0)$ | zero-loading $M$–$S$ diffusivity, m$^2$ s$^{-1}$ |
| $D_{i,Kn}$ | Knudsen diffusivity of species $i$, m$^2$ s$^{-1}$ |
| $Đ_{ii}$ | self-exchange coefficient, m$^2$ s$^{-1}$ |
| $Đ_{12}$ | $M$–$S$ exchange coefficient for binary mixture, m$^2$ s$^{-1}$ |
| $-\Delta H_{st}$ | isosteric heat of adsorption, J mol$^{-1}$ |
| $l$ | thickness of membrane, m |
| $M_i$ | molar mass of species $i$, kg mol$^{-1}$ |
| $n$ | number of components in mixture |
| $N_i$ | molar flux of species $i$ defined in terms of the membrane area, mol m$^{-2}$ s$^{-1}$ |
| $p_{i0}$ | partial pressure of species $i$ in upstream compartment, Pa |
| $p_{il}$ | partial pressure of species $i$ in downstream compartment, Pa |
| $p_t$ | total system pressure in upstream compartment, Pa |
| $q_i$ | molar loading species $i$ |
| $R$ | gas constant, 8.314 J mol$^{-1}$ K$^{-1}$ |
| $S_{ads}$ | adsorption selectivity |
| $S_{diff}$ | diffusion selectivity |
| $S_{perm}$ | permeation selectivity |
| $T$ | temperature, K |
| $V_p$ | accessible pore volume, m$^3$ kg$^{-1}$ |
| $x_i$ | mole fraction of species $i$ based on loading within pore |
| $z$ | distance along the membrane, m |

*Greek letters*

| | |
|---|---|
| $\Gamma_{ij}$ | thermodynamic factors, dimensionless |
| $\phi$ | fractional pore volume, dimensionless |
| $\mu_i$ | molar chemical potential, J mol$^{-1}$ |
| $\Pi_i$ | permeance of species $i$, mol m$^{-2}$ s$^{-1}$ Pa$^{-1}$ |
| $\theta_i$ | fractional occupancy of component $i$, dimensionless |

*Subscripts*

| | |
|---|---|
| 0 | referring to upstream face of membrane |
| $l$ | referring to downstream face of membrane |
| $i$ | referring to component $i$ |
| $p$ | referring to pore |
| $t$ | referring to total mixture |
| $Kn$ | referring to Knudsen |

## References

[1] M. Eddaoudi, J. Kim, N. Rosi, D. Vodak, J. Wachter, M. O'Keeffe, O.M. Yaghi, Systematic design of pore size and functionality in isoreticular MOFs and their application in methane storage, Science 295 (2002) 469–472.
[2] R. Banerjee, H. Furukawa, D. Britt, C. Knobler, M. O'Keeffe, O.M. Yaghi, Control of pore size and functionality in isoreticular zeolitic imidazolate frameworks and their carbon dioxide selective capture properties, J. Am. Chem. Soc. 131 (2009) 3875–3877.
[3] R. Banerjee, A. Phan, B. Wang, C. Knobler, H. Furukawa, M. O'Keeffe, O.M. Yaghi, High-throughput synthesis of zeolitic imidazolate frameworks and application to $CO_2$ capture, Science 319 (2008) 939–943.
[4] G. Férey, Hybrid porous solids: past, present, future, Chem. Soc. Rev. 37 (2008) 191–214.
[5] A.U. Czaja, N. Trukhan, U. Müller, Industrial applications of metal–organic frameworks, Chem. Soc. Rev. 38 (2009) 1284–1293.
[6] J.R. Li, R.J. Kuppler, H.C. Zhou, Selective gas adsorption and separation in metal–organic frameworks, Chem. Soc. Rev. 38 (2009) 1477–1504.
[7] R.J. Kuppler, D.J. Timmons, Q.R. Fang, J.R. Li, T.A. Makal, M.D. Young, D. Yuan, D. Zhao, W. Zhuang, H.C. Zhou, Potential applications of metal–organic frameworks, Coord. Chem. Rev. 253 (2009) 3042–3066.
[8] K.A. Cychosz, R. Ahmad, A.J. Matzger, Liquid phase separations by crystalline microporous coordination polymers, Chem. Sci. 1 (2010) 293–302.
[9] D.M. D'Alessandro, B. Smit, J.R. Long, Carbon dioxide capture: current trends and prospects for new materials, Angew. Chem. Int. Ed. 49 (2010) 6058–6082.
[10] S.T. Meek, J.A. Greathouse, M.D. Allendorf, Metal–organic frameworks: a rapidly growing class of versatile nanoporous materials, Adv. Mater. 23 (2011) 249–267.

[11] S. Keskin, T.M. van Heest, D.S. Sholl, Can metal–organic framework materials play a useful role in large-scale carbon dioxide separations? ChemSusChem 3 (2010) 879–891.
[12] G. Férey, C. Serre, T. Devic, G. Maurin, H. Jobic, P.L. Llewellyn, G. De Weireld, A. Vimont, M. Daturi, J.S. Chang, Why hybrid porous solids capture greenhouse gases? Chem. Soc. Rev. 40 (2011) 550–562.
[13] R. Krishna, J.M. van Baten, In silico screening of zeolite membranes for $CO_2$ capture, J. Membr. Sci. 360 (2010) 323–333.
[14] R. Krishna, J.M. van Baten, In silico screening of metal–organic frameworks in separation applications, Phys. Chem. Chem. Phys. (2011), http://dx.doi.org/10.1039/C1CP20282K.
[15] D. Britt, H. Furukawa, B. Wang, T.G. Glover, O.M. Yaghi, Highly efficient separation of carbon dioxide by a metal–organic framework replete with open metal sites, Proc. Natl. Acad. Sci. U.S.A. 106 (2009) 20637–20640.
[16] N.L. Rosi, J. Kim, M. Eddaoudi, B. Chen, M. O'Keeffe, O.M. Yaghi, Rod packings and metal–organic frameworks constructed from rod-shaped secondary building units, J. Am. Chem. Soc. 127 (2005) 1504–1518.
[17] P.D.C. Dietzel, B. Panella, M. Hirscher, R. Blom, H. Fjellvåg, Hydrogen adsorption in a nickel based coordination polymer with open metal sites in the cylindrical cavities of the desolvated framework, Chem. Commun. (2006) 959–961.
[18] P.D.C. Dietzel, V. Besikiotis, R. Blom, Application of metal–organic frameworks with coordinatively unsaturated metal sites in storage and separation of methane and carbon dioxide, J. Mater. Chem. 19 (2009) 7362–7370.
[19] S.R. Caskey, A.G. Wong-Foy, A.J. Matzger, Dramatic tuning of carbon dioxide uptake via metal substitution in a coordination polymer with cylindrical pores, J. Am. Chem. Soc. 130 (2008) 10870–10871.
[20] A.Ö. Yazaydın, R.Q. Snurr, T.H. Park, K. Koh, J. Liu, M.D. LeVan, A.I. Benin, P. Jakubczak, M. Lanuza, D.B. Galloway, J.J. Low, R.R. Willis, Screening of metal–organic frameworks for carbon dioxide capture from flue gas using a combined experimental and modeling approach, J. Am. Chem. Soc. 131 (2009) 18198–18199.
[21] Z. Bao, L. Yu, Q. Ren, X. Lu, S. Deng, Adsorption of $CO_2$ and $CH_4$ on a magnesium-based metal organic framework, J. Colloid Interface Sci. 353 (2011) 549–556.
[22] L. Hamon, E. Jolimaitre, G. Pirngruber, $CO_2$ and $CH_4$ separation by adsorption using Cu-BTC metal–organic framework, Ind. Eng. Chem. Res. 49 (2010) 7497–7503.
[23] Z.R. Herm, J.A. Swisher, B. Smit, R. Krishna, J.R. Long, Metal–organic frameworks as adsorbents for hydrogen purification and pre-combustion carbon dioxide capture, J. Am. Chem. Soc. 133 (2011) 5664–5667.
[24] M. Gallo, D. Glossman-Mitnik, Fuel gas storage and separations by metal–organic frameworks: simulated adsorption isotherms for $H_2$ and $CH_4$ and their equimolar mixture, J. Phys. Chem. C 113 (2009) 6634–6642.
[25] S. Keskin, Comparing performance of CPO and IRMOF membranes for gas separations using atomistic models, Ind. Eng. Chem. Res. 49 (2010) 11689–11696.
[26] S. Keskin, D.S. Sholl, Screening metal–organic framework materials for membrane-based methane/carbon dioxide separations, J. Phys. Chem. C 111 (2007) 14055–14059.
[27] S. Keskin, D.S. Sholl, Assessment of a metal–organic framework membrane for gas separations using atomically detailed calculations: $CO_2$, $CH_4$, $N_2$, $H_2$ mixtures in MOF-5, Ind. Eng. Chem. Res. 48 (2009) 914–922.
[28] S. Keskin, D.S. Sholl, Efficient methods for screening of metal organic framework membranes for gas separations using atomically detailed models, Langmuir 25 (2009) 11786–11795.
[29] S. Keskin, D.S. Sholl, Selecting metal organic frameworks as enabling materials in mixed matrix membranes for high efficiency natural gas purification, Energy Environ. Sci. 3 (2010) 343–351.
[30] S. Keskin, Molecular simulation study of $CH_4/H_2$ mixture separations using metal–organic framework membranes and composites, J. Phys. Chem. C 114 (2010) 13047–13054.
[31] H. Bux, C. Chmelik, R. Krishna, J. Caro, Ethene/ethane separation by the MOF membrane ZIF-8: molecular correlation of permeation, adsorption, diffusion, J. Membr. Sci. 369 (2011) 284–289.
[32] H. Bux, C. Chmelik, J.M. Van Baten, R. Krishna, J. Caro, Novel MOF-membrane for molecular sieving predicted by IR-diffusion studies and molecular modeling, Adv. Mater. 22 (2010) 4741–4743.
[33] Y.S. Li, F.Y. Liang, H. Bux, A. Veldhoff, W.S. Yang, J. Caro, Molecular sieve membrane: supported metal–organic framework with high hydrogen selectivity, Angew. Chem. Int. Ed. 49 (2010) 548–551.
[34] R. Krishna, J.M. van Baten, Unified Maxwell–Stefan description of binary mixture diffusion in micro- and meso-porous materials, Chem. Eng. Sci. 64 (2009) 3159–3178.
[35] R. Krishna, Describing the diffusion of guest molecules inside porous structures, J. Phys. Chem. C 113 (2009) 19756–19781.
[36] R. Krishna, J.M. van Baten, A simplified procedure for estimation of mixture permeances from unary permeation data, J. Membr. Sci. 367 (2011) 204–210.
[37] R. Krishna, J.M. van Baten, Highlighting pitfalls in the Maxwell–Stefan modeling of water–alcohol mixture permeation across pervaporation membranes, J. Membr. Sci. 360 (2010) 476–482.
[38] R. Krishna, J.M. van Baten, Segregation effects in adsorption of $CO_2$ containing mixtures and their consequences for separation selectivities in cage-type zeolites, Sep. Purif. Technol. 61 (2008) 414–423.
[39] R. Krishna, J.M. van Baten, Mutual slowing-down effects in mixture diffusion in zeolites, J. Phys. Chem. C 114 (2010) 13154–13156.
[40] R. Krishna, J.M. van Baten, Insights into diffusion of gases in zeolites gained from molecular dynamics simulations, Micropor. Mesopor. Mater. 109 (2008) 91–108.
[41] R. Krishna, J.M. van Baten, Onsager coefficients for binary mixture diffusion in nanopores, Chem. Eng. Sci. 63 (2008) 3120–3140.
[42] O. Talu, A.L. Myers, Molecular simulation of adsorption: Gibbs dividing surface and comparison with experiment, AIChE J. 47 (2001) 1160–1168.
[43] A.L. Myers, P.A. Monson, Adsorption in porous materials at high pressure: theory and experiment, Langmuir 18 (2002) 10261–10273.
[44] R. Krishna, J.M. van Baten, Describing mixture diffusion in microporous materials under conditions of pore saturation, J. Phys. Chem. C 114 (2010) 11557–11563.
[45] R. Krishna, J.M. van Baten, Investigating cluster formation in adsorption of $CO_2$, $CH_4$, and Ar in zeolites and metal organic frameworks at sub-critical temperatures, Langmuir 26 (2010) 3981–3992.
[46] R Krishna, J.M. van Baten, Highlighting a variety of unusual characteristics of adsorption and diffusion in microporous materials induced by clustering of guest molecules, Langmuir 26 (2010) 8450–8463.
[47] R. Krishna, J.M. van Baten, Hydrogen bonding effects in adsorption of water–alcohol mixtures in zeolites and the consequences for the characteristics of the Maxwell–Stefan diffusivities, Langmuir 26 (2010) 10854–10867.
[48] R. Krishna, J.M. van Baten, An investigation of the characteristics of Maxwell–Stefan diffusivities of binary mixtures in silica nanopores, Chem. Eng. Sci. 64 (2009) 870–882.
[49] R. Krishna, J.M. van Baten, A molecular dynamics investigation of the unusual concentration dependencies of Fick diffusivities in silica mesopores, Micropor. Mesopor. Mater. 138 (2011) 228–234.
[50] R. Krishna, J.M. van Baten, Influence of adsorption on the diffusion selectivity for mixture permeation across mesoporous membranes, J. Membr. Sci. 369 (2011) 545–549.
[51] M.D. Foster, I. Rivin, M.M.J. Treacy, O.D. Friedrichs, A geometric solution to the largest-free-sphere problem in zeolite frameworks, Micropor. Mesopor. Mater. 90 (2006) 32–38.
[52] S.K. Bhatia, D. Nicholson, Some pitfalls in the use of the Knudsen equation in modelling diffusion in nanoporous materials, Chem. Eng. Sci. 66 (2011) 284–293.
[53] R. Krishna, Multicomponent surface diffusion of adsorbed species—a description based on the generalized Maxwell–Stefan equations, Chem. Eng. Sci. 45 (1990) 1779–1791.
[54] R. Krishna, R. Baur, Modelling issues in zeolite based separation processes, Sep. Purif. Technol. 33 (2003) 213–254.
[55] R. Krishna, J.M. van Baten, Diffusion of alkane mixtures in zeolites. Validating the Maxwell–Stefan formulation using MD simulations, J. Phys. Chem. B 109 (2005) 6386–6396.
[56] P.F. Lito, A.S. Santiago, S.P. Cardoso, B.R. Figueiredo, C.M. Silva, New expressions for single and binary permeation through zeolite membranes for different isotherm models, J. Membr. Sci. 367 (2011) 21–32.
[57] R. Krishna, J.M. van Baten, A molecular dynamics investigation of the diffusion characteristics of cavity-type zeolites with 8-ring windows, Micropor. Mesopor. Mater. 137 (2011) 83–91.
[58] A.L. Myers, J.M. Prausnitz, Thermodynamics of mixed gas adsorption, AIChE J. 11 (1965) 121–130.
[59] R. Krishna, S. Calero, B. Smit, Investigation of entropy effects during sorption of mixtures of alkanes in MFI zeolite, Chem. Eng. J. 88 (2002) 81–94.
[60] R. Krishna, J.M. van Baten, Using molecular simulations for screening of zeolites for separation of $CO_2/CH_4$ mixtures, Chem. Eng. J. 133 (2007) 121–131.
[61] R. Krishna, D. Paschek, R. Baur, Modelling the occupancy dependence of diffusivities in zeolites, Micropor. Mesopor. Mater. 76 (2004) 233–246.
[62] R. Krishna, R. Baur, Diffusion, Adsorption and Reaction in Zeolites: Modelling and Numerical Issues, University of Amsterdam, Amsterdam, http://www.science.uva.nl/research/cr/zeolite/, 11 November 2003.
[63] S. Li, J.L. Falconer, R.D. Noble, R. Krishna, Interpreting unary, binary and ternary mixture permeation across a SAPO-34 membrane with loading-dependent Maxwell–Stefan diffusivities, J. Phys. Chem. C 111 (2007) 5075–5082.
[64] R. Krishna, S. Li, J.M. van Baten, J.L. Falconer, R.D. Noble, Investigation of slowing-down and speeding-up effects in binary mixture permeation across SAPO-34 and MFI membranes, Sep. Purif. Technol. 60 (2008) 230–236.
[65] J.C. White, P.K. Dutta, K. Shqau, H. Verweij, Synthesis of ultrathin zeolite Y membranes and their application for separation of carbon dioxide and nitrogen gases, Langmuir 26 (2010) 10287–10293.
[66] J. van den Bergh, W. Zhu, J. Gascon, J.A. Moulijn, F. Kapteijn, Separation and permeation characteristics of a DD3R zeolite membrane, J. Membr. Sci. 316 (2008) 35–45.
[67] Y. Li, F. Liang, H. Bux, W. Yang, J. Caro, Zeolitic imidazolate framework ZIF-7 based molecular sieve membrane for hydrogen separation, J. Membr. Sci. 354 (2010) 48–54.
[68] H. Bux, F. Liang, Y. Li, J. Cravillon, M. Wiebcke, J. Caro, Zeolitic imidazolate framework membrane with molecular sieving properties by microwave-assisted solvothermal synthesis, J. Am. Chem. Soc. 131 (2009) 16000–16001.